Eur. Phys. J. D **23**, 99–107 (2003)
DOI: 10.1140/epjd/e2003-00010-4

THE EUROPEAN PHYSICAL JOURNAL D

Production of high quality shocks for equation of state experiments

D. Batani[1,a], F. Strati[1], B. Telaro[1], Th. Löwer[2,b], T. Hall[3], A. Benuzzi-Mounaix[4], and M. Koenig[4]

[1] Dipartimento di Fisica "G. Occhialini", Università degli Studi di Milano-Bicocca, and INFM, Piazza della Scienza 3, 20126 Milano, Italy
[2] Max Planck Institut für Quantenoptik, 85740 Garching, Germany
[3] University of Essex, Wivenhoe Park, Colchester CO 3SQ, UK
[4] Laboratoire pour l'Utilisation des Lasers Intenses (LULI)[c], CNRS-CEA-X-Paris VI, École Polytechnique, 91128 Palaiseau, France

Received 17 June 2002
Published online 21 January 2003 –

Abstract. In this paper we describe the quality requirements that a shock wave must fulfil to make equation of state (EOS) measurements possible: planarity, no-preheating and stationarity of the shock. Experimental measurements have been performed at the Max Planck Institut für Quantenoptik (Garching). We also present simple analytical models that allow to verify shock stationarity and absence of preheating.

PACS. 52.50.Jm Plasma production and heating by laser beams (laser-foil, laser-cluster, etc.) – 52.35.Tc Shock waves and discontinuities

1 Introduction

In recent years, laser driven shock waves have begun to be an usable tool in high pressure physics, in particular in experiments for the determination of Equation of State (EOS) of materials at Megabar pressures. The principle of shock formation is quite simple: when a high energy laser pulse is focused on the surface of a solid material, it induces a rapid ablation of its surface layers. As a consequence of Newton's third law of dynamics (principle of action and reaction), the rest of the material is pushed inside (rocket effect) creating a shock wave which compresses the material. This allows very high pressures to be obtained (Megabar range). In particular it is found that the shock pressure is related to laser and target parameters by the well known scaling law [1]

$$P(\text{Mbar}) = 11.6\left(I_{\text{L}}/10^{14}\right)^{3/4} \times \lambda^{-1/4}(A/2Z)^{7/16}\left(\frac{Z^*}{3.5}t\right)^{-1/8} \quad (1)$$

where A and Z are the mass number and the atomic number of the target, I_{L} is the laser intensity on target in W/cm^2, λ is the wavelength in μm and t is the time in ns. The pressure strongly depends on laser parameters and only weakly on target parameters. Also shock pressure tends to decrease in time even for a constant laser irradiation. This fact is due to the increasing separation between the ablation surface ($n_e \approx$ solid material) and the layer where the laser beam is absorbed, and has been first described in the papers by Caruso and Gratton [2] and Mora [1].

Let's note that very often scaling laws without a temporal dependence are reported in literature, even in recent reviews [3]:

$$P = 8.6(I_{\text{L}}/10^{14})^{2/3}\lambda^{-2/3}(A/2Z)^{1/3}. \quad (2)$$

These must be considered only as an approximation giving the order of magnitude, while the correct scaling-law includes the time dependence.

However, usually, laser produced shocks have a "poor" quality, a fact which has long prevented their use as a quantitative tool in high pressure physics. Shock wave EOS experiments are based on the use of Rankine-Hugoniot equations which, in the limits of very strong shocks, are [4]:

$$\begin{cases} \rho(D-u) = \rho_0 D \\ P - P_0 = \rho_0 D u \\ E - E_0 = u^2/2 \end{cases} \quad (3)$$

and respectively represents the conservation of mass, momentum and energy across the shock front. In these equations ρ is the density, D the shock velocity, u the fluid

[a] e-mail: batani@mib.infn.it
[b] *Present address*: Pro-beam, Behrinstaße 6, 85152 Planegg b. München, Germany.
[c] UMR 7605

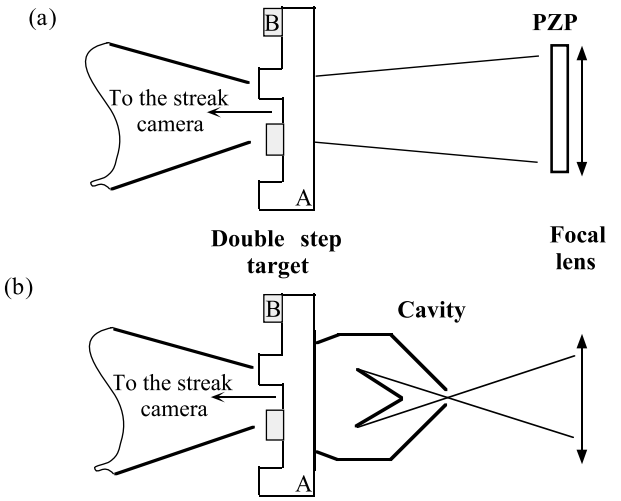

Fig. 1. Experimental set-up at MPQ. PZPs (a) and cavities (b) are used for production of high quality shocks.

velocity in the compressed material, P the pressure and E the internal energy. The suffix 0 indicates the unperturbed condition. A point on the EOS of the material (P, ρ, E) is determined through the experimental measurements of some parameters (like the shock and/or fluid velocity in the compressed material) and the knowledge of the parameters of the uncompressed material (P_0, ρ_0, E_0).

These equations are 1D, hence they require a planar shock (uniform pressure along the shock front). Moreover shock velocity must be constant in time. Finally they require the absence of any perturbation (preheating) before the shock front which changes the values of (P_0, ρ_0, E_0).

In the following, we will discuss in more detail these quality requirements. In particular, we will refer to laser driven shock wave experiments done with "two steps-two materials" targets [5,6]. These allow "relative" measurements of EOS. The EOS point of an "unknown" material is determined using a material with known EOS as a reference and by comparing the shock velocity in the two materials (*i.e.* in the two steps).

2 Experimental set-up

The experiment was performed using the asterix iodine laser of the Max Planck Institut für Quantenoptik, which delivers a single beam, 30 cm in diameter, with typical energy of 250 J per pulse at a wavelength of 0.44 μm. The temporal behaviour of the laser pulse is Gaussian with a Full Width at Half Maximum (FWHM) of 450 ps. In order to generate the shock wave into the target, we used both direct and indirect laser drive. Figure 1 shows the two different schematic experimental set-ups.

The focusing lens had a focal length $f = 564$ mm lens ($f/2$ aperture).

The diagnostic used to detect the shock breakout from the target rear face consisted in a pair of lenses imaging the rear face onto the slit of a streak camera, working in the visible region. The first one was a $f/2$ objective, with a focal length $f = 100$ mm, producing a parallel beam between the two lenses. The system temporal resolution was better than 8 ps and the imaging magnification was $M = 10$, allowing a spatial resolution better than 10 μm. A protection system [5] was used to shield the diagnostic light path and the streak camera from scattered laser light.

Targets were made of aluminium (reference material) and another "unknown" material (gold or copper in our experiment [5,6]) and produced at the Laboratoire des Cibles of the Commissariat l'Énergie Atomique, Limeil-Valenton. The accurate fabrication technique [7] allowed sharp step edges and a precise determination of step heights. The Al base was ≈10 μm, and the steps thickness ≈6 μm for Al and ≈3 and 4 μm for Au [6] and for Cu respectively [5].

On some targets there was an additional plastic (CH) layer. The laser was then focused on a low Z material (CH) producing low X-ray emission and reducing preheat (see Sect. 4.1) and hence satisfying the third quality requirement.

3 Planarity

Planarity is strongly related to the homogeneity of the energy deposition on the target, and therefore to the spatial homogeneity of the laser beam. The spatial profile of the pressure obtained on the target reflects the laser intensity profile. Hence there are two aspects connected to planarity: homogeneity on small scales and homogeneity on large scales.

The first refers to the absence of laser hot spots in the beam, *i.e.* localised high intensity regions which would produce localised early shock breakouts.

The second one refers to the overall shape of the laser intensity distribution and of the shock front.

The problem of small scale inhomogeneities may be solved by using optical smoothing techniques like Random Phase Plates (RPP) [8], Phase Zone Plates (PZP) [9,10], or Kinoform Phase Plates (KPP) [11]. However RPPs give a global envelop of the intensity distribution which is close to Gaussian. In this case we get a maximum pressure in the centre, and then the pressure decreases on the edges: if the pressure changes point by point, its measurement will then be more difficult. To obtain a planar profile of the shock, it is necessary to use PZP or KPP [9–11] or, alternatively, to use holhraums and the indirect drive technique. In our experiments we used both holhraums and PZPs (the practical use of KPP is similar to PZP, even if their optical principle is different). We will describe results obtained both with direct drive with PZP and results obtained with indirect drive and holhraums.

3.1 Planarity in direct drive

Phased Zone Plates are a bidimensional array of Fresnel lenses etched on a glass slab. These are disposed so to

randomly introduce phase differences of 0 or π on the wave front of the laser. This breaks the spatial coherence of the laser beam and produces a smooth intensity profile [9,10].

A Fresnel lens is a set of concentric zones (Fresnel zones), alternatively introducing a 0 or π phase difference on the incident beam: the total phase difference given by a lens depends on the phase of the central zone. Fresnel lenses exactly behave as lenses, with a focal distance $f_1 = R_1^2/\lambda$, where R_1 is the central zone radius and λ is the wavelength of the beam. The diameter of the Fresnel lens is $w = 2m^{1/2}$, where m is the number of Fresnel zones in the lens.

The working principle of PZP is the following. The PZP is used together with a normal lens of focal length f. The laser beam invests the focusing lens and the PZP, which divides it in a large number of beamlets. These will be focused in a plane determined by the total focal length of the optical system $f_{\rm tot}$ (being $1/f_{\rm tot} = 1/f + 1/f_1$). Each beam will be focused in different points of this plane. Instead at distance f, *i.e.* on the focal plane of the principal lens, one will obtain a superposition of the beamlets. The diameter of the spot formed in this plane is $\Phi = wf/f_1 = 4m\lambda f/w$.

At distance f the intensity distribution is not plane but characterised by the presence of a central peak (due to various effects described in [9,10,12,13]). A slightly defocusing of the system (obtained by moving the target out of the focal plane) makes the peak to disappear giving a super-Gaussian intensity distribution. A larger defocusing produces instead a Gaussian-like shape of intensity like in the case of RPP.

The conditions for the PZP to produce good optical smoothing are:

- the laser beam has to invest a large number of Fresnel lenses to optimise the homogenisation effect;
- each Fresnel lens must contain many Fresnel zones to optimise the focusing power (which implies that each Fresnel lens must not be too small).

Hence the asterix beam is particularly suitable to be optically smoothed with PZP due to its large diameter (Φ = 29 cm). The Fresnel lenses were characterised by w = 2.5 cm and R_1 = 4.17 mm. Hence f_1 = 3 964 cm, m = 9 and approximately $(\Phi/w)^2 \approx 130$ Fresnel lenses were contained in the laser beam.

Figure 2 shows some examples of shock breakout obtained with different planarities, depending on the position of the target with respect to the PZP. Specifically, Figure 2a has been obtained with the target in the focal plane of the main focusing lens (distance f) and shows the central peak. Figure 2b corresponds to the optimal position of PZP (flat intensity distribution, planar shock). Figure 2c corresponds to a large defocusing and gives a curved shock front. Finally Figure 2d corresponds to PZP whose etched features had a reduced thickness, not enough to introduce a π dephasing. In this case, an Airy pattern is superimposed to the flat-top intensity distribution: the Airy rings are clearly visible in the shock breakout profile.

The best case (Fig. 2b) allows a direct comparison with analytical models and 1D hydrodynamical simulations.

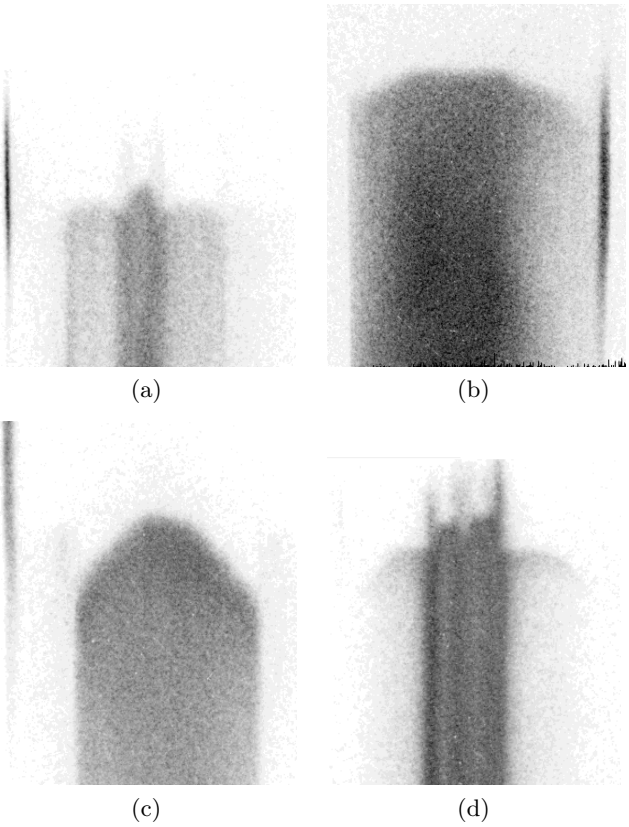

Fig. 2. Shock breakout images obtained with the streak camera. The target positions is varied relatively to the focal plane. In all cases the laser energy was $E_{\rm L} \approx 250$ J corresponding to $I_{\rm L} \approx 2.5 \times 10^{14}$ W/cm^2. The horizontal axis is space, the vertical axis time. Time flows up to down. The dimensions of the image are about 700 μm $\times$ 2.5 ns. (a) Shock with a central peak (3 μm Au target, focal position: 564 mm from the lens); (b) shock with a planar profile (3 μm Au target, position with respect to the focus +160 μm); (c) shock with a Gaussian profile (18 μm Al target, position with respect to the focus + 400 μm); (d) shock with an Airy spot profile (18 μm Al target, focal position: 564 mm from the lens).

In this case the planarity measured along the shock front was $\pm$5 ps, *i.e.* the shock breaks out with a time delay of $\pm$5 ps in different target positions (of course we refer to the central part of the focal spot only, with planar intensity distribution). This is very close to the streak camera temporal resolution ($\leq$8 ps). In our experiment typical values of laser and shock parameters were $I_{\rm L} = 2 \times 10^{14}$ W/cm^2, P = 26 Mbar and D = 36 μm/ns. Hence, using a target with typical thickness d = 5 μm, a value $\Delta t = \pm 5$ ps implies $\Delta D = \pm 1.3$ μm/ns or $\Delta D/D = 3.6\%$. This of course imposes a limit on accuracy to which EOS data can be obtained. With the indirect drive a slightly better planarity was achieved, at the cost of a reduced energy coupling (see next section).

Even if these results are quite good, in principle they could be related to the diagnostic (streak camera) resolution. Evidencing localised early shock breakout from laser

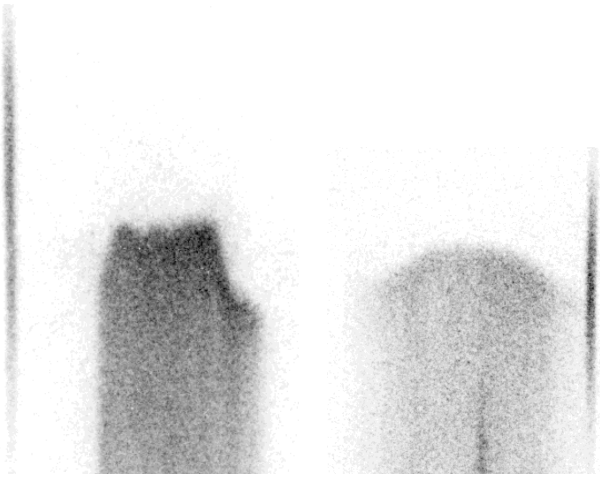

(a) (b)

Fig. 3. Comparison between streak-camera images obtained with: (a) 18 μm Al target ($E_{\rm L}$ = 245 J); (b) 3 μm Au target ($E_{\rm L}$ = 214 J). The horizontal axis is space, the vertical axis time. Time flows up to down. The dimensions of the image are about 700 μm × 2.5 ns.

speckles could require better space and time resolution. To this goal a recent experiment was realised at LULI, and presented in [14], which used the "Chirped Beam Reflectivity" diagnostic to measure shock breakout with space and time resolution of 8 μm and 1 ps respectively. In this experiment the spiky structure in the focal spot was evidenced, but differences in shock arrival time across the shock front did not exceed ±10 ps (also optical smoothing in that case was not optimised as in the experiment at MPQ).

Finally Figure 3 compares streak-camera images obtained in a 18 μm Al target, Figure 3a, and in a 3 μm Au target, Figure 3b (let's observe that the areal density of the targets are close, since $\rho_{\rm Al}$ = 2.7 g/cm^3 and $\rho_{\rm Au}$ = 19.3 g/cm^3). The breakout profile obtained in Al is more planar than with Au in similar conditions. We suppose that is due to a stronger thermal smoothing in Al (and to the larger target thickness implying a larger geometrical smoothing). Indeed due to the lower atomic number (Z) and mass density (ρ) the temperature reached in Al can be larger [15]. With this respect, let's notice that sometimes images of shock breakout presented to show planarity are obtained with CH targets [16] implying an increased thermal smoothing. We think that such images are not conclusive and that harder materials should be used in this context.

3.2 Planarity in indirect drive

In this case, the shock wave is generated using thermal X-rays from laser-heated cavities. Planarity is a consequence of the homogeneity of Planckian radiation. In the experiments we focused the laser beam into a 1-mm-size gold cavity through a small entrance hole. When the laser is focused in the cavity, an isotropic radiation is created [17] whose temperature depends upon the cavity size and the laser power. The temperature of the cavity can be determined by observing the velocity of a shock wave generated when radiation is absorbed in low-Z material [18]. With our experimental set-up, this has been measured to be in the range of 100–150 eV.

The planarity achieved by indirect drive is shown in Figure 4c. The profile of the rearside emission is smoother than with direct drive. But the slight improvement in the uniformity of energy deposition is obtained at the cost of an important energy loss. Indeed in this case pressure generated on target is related to the cavity radiation temperature and hence to cavity size and laser intensity through the formula

$$P_{\rm ind}({\rm Mbar}) = 44(I_{\rm C}/10^{14})^{10/13} t^{-3/26} \tag{4}$$

here t is time (in ns), $I_{\rm C}$ is the X-ray intensity on target in W/cm^2 [3,17,18]:

$$I_{\rm C} = \frac{\eta E_{\rm L}}{4\pi R_{\rm C}^2 \tau_X} \tag{5}$$

η is the efficiency conversion of laser energy in primary X-rays, $R_{\rm C}$ is the radius of the cavity and $\tau_{\rm X}$ the duration of the X-ray pulse (which is comparable to the laser pulse duration $\tau_{\rm L}$). Comparing equation (4) and equation (1) and using $t = \tau_{\rm L}$ in order to get the order of magnitude, we obtain

$$E_{\rm ind} = \frac{0.61}{\eta}\left(\frac{Z^*}{3.5}\right)^{-0.162}\left(\frac{A}{2Z}\right)^{0.569} \times \frac{R_{\rm C}^2}{R^{1.95}}\left(\frac{E_{\rm dir}^3}{\lambda}\right)^{0.325}\tau_{\rm L}^{1/80} \tag{6}$$

which gives the energy needed in indirect drive to obtain the same pressure of direct drive. Here R and $R_{\rm C}$ are in μm, $E_{\rm ind}$ and $E_{\rm dir}$ in joules and $\tau_{\rm L}$ in ns. With our typical parameters ($E_{\rm dir}$ = 250 J, $R_{\rm C}$ = 500 μm, R = 200 μm, λ = 0.438 μm and $\tau_{\rm L}$ = 0.45 ns) we find a ratio $E_{\rm ind}/E_{\rm dir} \approx 5$. Hence in order to achieve the same shock pressure, a laser energy ≈5 times larger is needed in indirect drive.

If instead we use the approximate scaling law (2) we get

$$E_{\rm ind} = \frac{0.21}{\eta}\left(\frac{A}{2Z}\right)^{0.433}\frac{R_{\rm C}^2}{R^{1.73}}\left(\frac{E_{\rm dir}}{\lambda}\right)^{0.87}\tau_{\rm L}^{0.284} \tag{7}$$

as reported in [5]. In the two cases the ratio is practically the same because the numerical results from formulas (1) and (2) are close. For instance, using again $t = \tau_{\rm L}$ and the typical parameters of our experiment, we get P = 26.5 Mbar from (1) and P = 23.7 Mbar from (2).

4 Pre-heating of the target

Pre-heating consists in matter being warmed up before shock arrival. It is a crucial problem in shock EOS experiments which are based on the use of Rankine-Hugoniot

equations (Eq. (3)). If targets are pre-heated, the material is no longer unperturbed before the arrival of the shock and the parameters of the material ahead of the shock front become unknown.

Pre-heating may be detected by an early luminosity emerging from the target rear-side before shock arrival. The increase in temperature may indeed be sufficient to cause some emission in the visible and infrared regions before shock breakout. After shock breakout an important heating of the material will imply a slower decay of rear side luminosity (the connection between preheating and backside emission has been studied experimentally in Refs. [19–21] and numerically in [21,22]).

In our experiment, both with direct and indirect drive, we can exclude a significant preheating by looking at the temporal shape of the rear-side luminescence, characterized by a fast decay and an even faster rise time.

Recent experiments have shown that other diagnostic methods based on reflectivity [14] or interferometric measurements [12] are more sensitive to the presence of preheating. However these were not implemented in the present experiment due to the non availability of a probe laser beam.

4.1 Pre-heating in direct drive

In direct drive, pre-heating can be due to different causes:

- supra-thermal electrons generated near the critical density by resonant absorption;
- supra-thermal electrons generated in the corona by laser supraintensities (possibly produced or amplified by the filamentation instability);
- "hard" X rays produced in the plasma corona.

The first phenomenon is reduced using a short wavelength laser and sufficiently low intensity (in our case $\lambda = 438$ nm and $I \approx 2 \times 10^{14}$ W/cm^2) [17,21], indeed it is well-known that resonant absorption is effective at intensities larger than $10^{14}/\left[\lambda(\mu\mathrm{m})^2\right]$ W/cm^2 [23]. The second effect is strongly reduced thanks to the use of optical smoothing techniques.

Hence in our experiment the main concern to preheating comes from X-rays from the corona. A simple analytical model can be used to evaluate preheating by quantifying the X-ray intensity produced in laser-plasma interaction. Following Batani *et al.* [12] and Lwer *et al.* [20], the preheating temperature produced on target rearside by the flux of photons with energy $h\nu$ is:

$$T(\nu, h) = S(\nu, h)\frac{\tau\mu(\nu)}{\rho C_{\mathrm{V}}} \tag{8}$$

where $S(\nu, h)$ is the X-ray intensity at distance h inside the target, τ is the X-pulse duration (of the order of the laser pulse duration), μ is the material absorption coefficient in cm^{-1}, ρ is the mass density and C_{V} the specific heat (for Al this is 0.9 J/g K if the temperature of the material is $\ll$1.5 eV and $\approx$1.7 J/g K in the range 1.5 eV $\leq T_{\mathrm{e}} \leq$ 3.5 eV [24]). Evaluating S as a function of laser energy we get for the temperature of the target rear side:

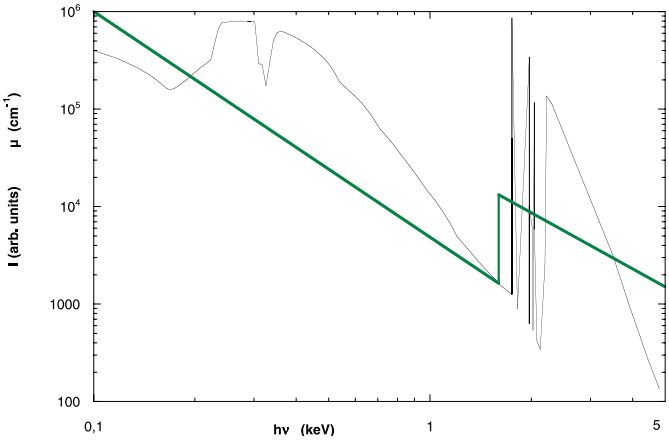

Fig. 4. Emission spectra of Al in X-ray region (solid line) in arbitrary units of intensity from reference [25]; absorption coefficient of Al in the same region in cm^{-1} from reference [26].

$$T = \frac{E_{\mathrm{L}}\mu\,\alpha\,\eta\,\mathrm{e}^{-\mu(\nu_0)d}}{\pi R^2 \rho\, C_{\mathrm{V}}} \tag{9}$$

where πR^2 is the area of the focal spot, d the target thickness, η the X-ray efficiency, and α represents the ratio of X-ray emitted towards the rearside of the target (we assume $\alpha = 1/2$). For Al, X-ray emission is centred around $h\nu \approx 500$ eV (L-shell emission) and $h\nu \approx 1.5$ keV (K-shell emission), as shown in Figure 4. The typical conversion efficiency in the two spectral bands are $\eta \approx 0.05$ and $\eta \approx 0.02$ respectively [25]. However X-rays around $h\nu \approx 500$ eV are very strongly absorbed in matter and will not reach the target rear side, hence will not give an appreciable contribution to preheating. We then concentrate on the harder keV spectral region and assume $\eta \approx 0.02$. In the region where X-ray emission is maximum, μ is always larger than 6×10^3 cm^{-1} (see Fig. 4) [26]. We consider such a value for our calculations. Actually the temperature found with (9) must be considered from a qualitative point of view because of the great uncertainty in the parameters involved. In the case of the MPQ experiment, with a $d = 10$ μm Al target, we find $T \approx 1$ eV, in agreement with what already reported in references [19,21].

The use of a CH layer on the laser side reduces preheating because:

(i) the laser to X-ray conversion efficiency η is lower in the case of plastic as compared to Al (due to the lower Z);
(ii) softer X-rays are produced in laser-plasma interaction in the case of plastic, which are then more effectively absorbed in the Al layer and do not contribute to preheating of the target rearside.

This is confirmed by the experimental results in Figures 5a and 5b which show streak camera images of shock breakouts obtained with Al/Au targets without (a) and with (b) a CH coating. Examples of time evolution of rearside luminosity are reported in Figures 6a for the case (a)

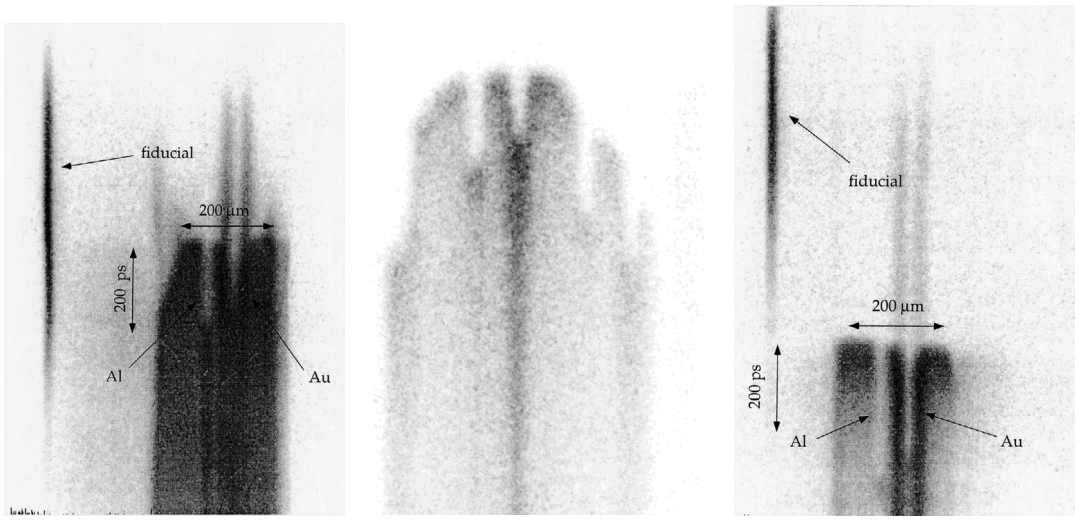

(a) (b) (c)

Fig. 5. Streak camera images of shocks obtained using different experimental set-ups. In all cases the Al base thickness was 10 μm and the Al step thickness was 6.23 μm: (a) direct drive + PZP + Al/Au targets ($E_{\mathrm{L}} = 293$ J), (b) direct drive + PZP + CH/Al/Au targets ($E_{\mathrm{L}} = 367$ J), (c) indirect drive + Al/Au targets ($E_{\mathrm{L}} = 290$ J).

and in Figures 6b and 6d for the case (b). The very rapid luminosity increase corresponds to the shock wave reaching the rear-side of the target. Before shock arrival, the rearside emission is negligible in the case of Figures 6b and 6d (CH layer) while it is evident in the case of Figure 6a (no CH coating).

From equation (9) we expect preheating to increase with laser energy. However a comparison of Figure 6b and 6c does not really show any significant increase in emission before shock breakout. Hence we can conclude that the use of a CH coating is very effective in reducing preheating. Of course the thickness of such layer must be chosen so that it is not completely ablated during the laser pulse.

Before closing the section, we notice that equation (9) is correct as long as the shock breaks out from rear-side after the end of the pulse, so that all the laser energy E_{L} contributes to shock production and preheating. With very thin targets, only the laser energy deposited before breakout contribute to preheating. This may reduce preheating with respect to what predicted by equation (9).

4.2 Preheating in indirect drive

In the case of indirect drive the presence of a CH layer is not useful to reduce preheating. Indeed the spectrum of the X-rays inside the cavity is thermal and is not influenced by the material of the cavity (and target) walls (at least once thermal equilibrium has been reached). Rather, in this case preheating is very sensitive to the geometry of the cavity. This was shown very well in the paper by Löwer *et al.* [20]. The problem arises because of the "primary" X-rays produced in the direct interaction of the beam with the cavity walls. This non-thermal harder X-rays may cause preheating whenever they reach the target.

Our cavity [24] has been designed not only to reach the high temperatures, recalled in the previous section (100–150 eV) but also to optimise uniformity when only one laser beam is used, and reduce preheating. Here, a shield with a conical shape has been constructed so that the laser irradiated area and the shocked material were not in direct view of each other, as shown in Figure 1b and the primary X-rays could not reach the target.

In this case preheating is negligible, as shown in Figures 4c and 6c: the second one, in particular, shows as the breakthrough emission rises very fast when the shock emerges from the target rearside, and in the previous instants is absolutely negligible.

5 Stationarity of the shock

The third fundamental quality requirement is stationarity: the velocity of the shock, while it goes through the target (or at least through the step), must be constant. This is a difficult requirement since the scaling laws (1) and (4) already predict shock pressure to fall with time. In order to overcome this difficulty a laser pulse with intensity increasing in time could be used, as for instance described in the numerical simulations in the paper by Temporal *et al.* [27]. However this makes the experiment difficult to be designed and realised, requiring laser pulse shaping. Luckily the dependence of D on t is weak enough ($D \approx t^{-1/16}$) so that shocks which are fairly constant in time are obtained with not-too-tick targets. Hence in the following we will not consider this point and focus on two other, more important, sources of non-stationarity.

The first cause of non stationarity is related to bidimensionality. This does not appear as long as the target thickness is small compared to the radius of the flat region of the intensity profile ($d \ll R$). If $d \geq R$ the shock

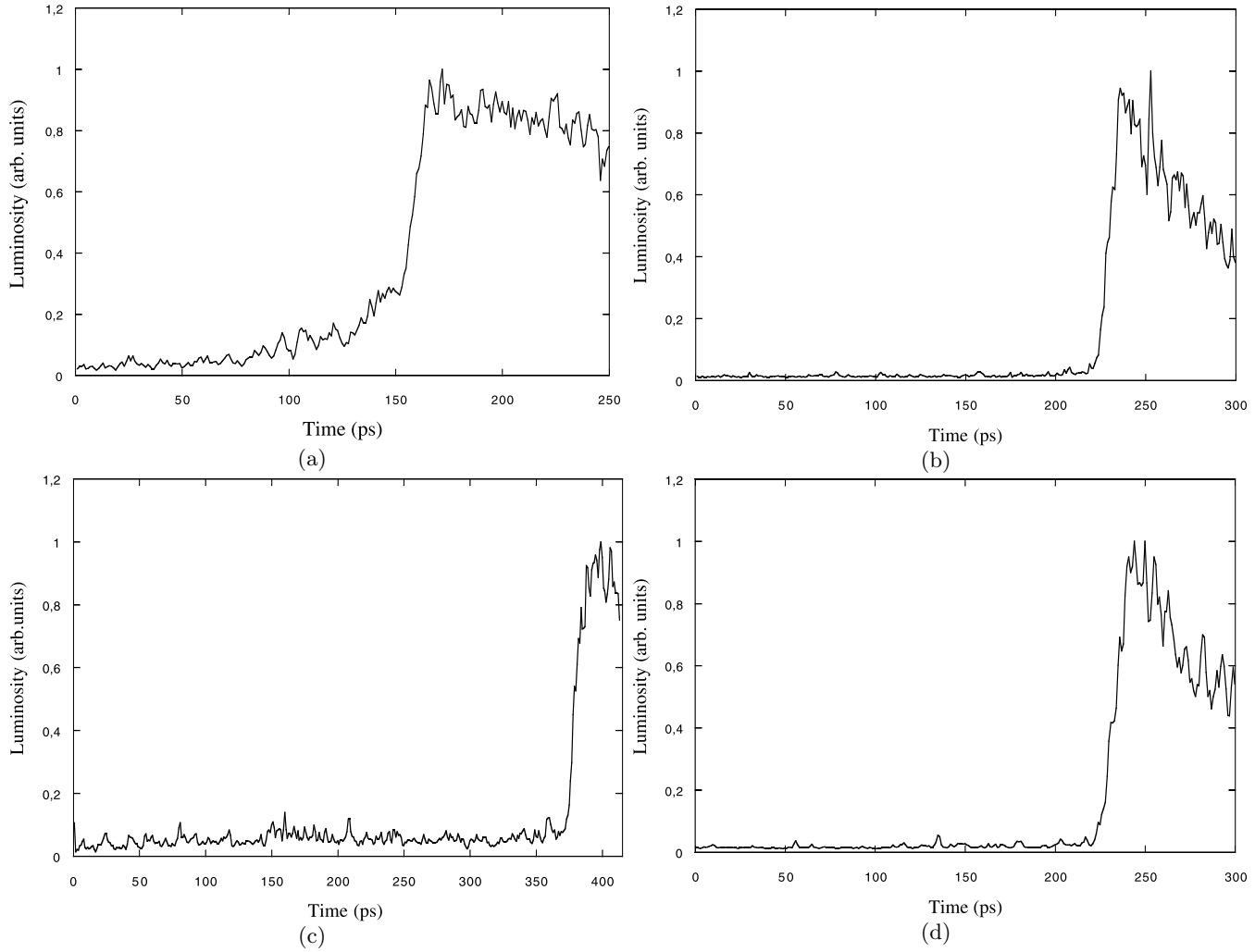

Fig. 6. Temporal evolution of the rear-side luminescence on the Al base. In all cases the signals are normalised to their maximum value; (a) direct drive and Al/Au target (the same of Fig. 4a) ($E_{\rm L} = 293$ J), (b) direct drive and CH/Al/Au target, low laser energy ($E_{\rm L} = 71$ J), (c) indirect drive and Al/Au target (the same of Fig. 4c) ($E_{\rm L} = 290$ J), (d) direct drive and CH/Al/Au target ($E_{\rm L} = 367$ J).

wave becomes spherical, and the pressure decreases as $P \approx P_0(R/d)^2$. In the case of our experiment at MPQ the thickness of the target was about 20 μm, while the diameter of the flat region was about 400 μm, hence 2D effects were negligible.

In the case $R \gg d$ (2D effects negligible), the shock may become non stationary due to the dynamics of shock and relaxation waves. Indeed:

(1) the early phase of shock formation is characterized by an increase in pressure with time (*i.e.* with space as the shock propagates in the material). Indeed the temporal trend of the shock pressure follows the laser intensity which is increasing in time. Hence to be stationary, the shock must already have reached its maximum value when it emerges from the target rearside;
(2) at late times, the shock can be non stationary because when the laser pulse finishes, it can no longer sustain the ablation pressure. Then an unloading wave originates at the critical surface and goes travels the target at the sound speed $c_{\rm s}$ (in the material already compressed by the shock). This wave may eventually reach the shock before it emerges from rear-side. In this case, the shock pressure will be reduced and the shock will no longer be stationary.

In the following we will assume a trapezoidal laser pulse profile. This is an approximation (the temporal profile being Gaussian) but allows to simplify the calculations. We call $t_{\rm R}$ the "rise time" of the laser pulse (from 0 to the maximum of the laser intensity), and $t_{\rm L}$ the time at which the intensity starts to decrease. Since the pressure profile follows the laser intensity, at $t = t_{\rm R}$ the shock reaches its maximum pressure, while at $t = t_{\rm L}$ the unloading wave is generated.

During the first "acceleration" phase ($t < t_{\rm R}$) the shock velocity will increase, due to the pressure (and intensity) increase, and for simplicity we can then assume that

its motion is uniformly accelerated. We can then write

$$a = D/t_{\mathrm{R}} \tag{10}$$

where D is the maximum value of shock velocity (*i.e.* when it becomes stationary) and a the average acceleration. The position reached at time t_{R} is

$$d_{\min} = \frac{1}{2} a\, t_{\mathrm{R}}^2 = \frac{1}{2} D t_{\mathrm{R}}. \tag{11}$$

Therefore the shock will be stationary only if $d > d_{\min}$.

Now, let's consider the second condition of stationarity, *i.e.* late times. In this case, the shock may reach the target rearside after the end of the pulse and can become not stationary. Let's indicate by x_{s} the position of the shock in the target at the time t (where $t = 0$ is represents the start of the laser pulse). Then

$$x_{\mathrm{s}} = \frac{1}{2} D t_{\mathrm{R}} + D(t - t_{\mathrm{R}}) = D(t - t_{\mathrm{R}}/2). \tag{12}$$

The position x_r of the unloading wave is instead given by

$$x_r = c_{\mathrm{s}}(t - t_{\mathrm{L}}) \frac{\rho_0}{\rho} \tag{13}$$

where (ρ/ρ_0) is the compression factor corresponding to the shock pressure P. In the case of very strong shocks, $(\rho/\rho_0) \approx 4$ [4] and then the thickness of the target is reduced by a factor 4. The maximum time $t_{\max}$ that allows the shock to emerge from the rearside of the target without being reached by the unloading wave can be calculated by combining the relations (12) and (13):

$$t_{\max} = \frac{4 c_{\mathrm{s}} t_{\mathrm{L}} - D t_{\mathrm{R}}/2}{4 c_{\mathrm{s}} - D}. \tag{14}$$

Then the maximum target thickness $d_{\max}$ that allows to the shock to emerge from the rearside before being reached from the unloading wave is:

$$d_{\max} = \frac{4 c_{\mathrm{s}} D (t_{\mathrm{L}} - t_{\mathrm{R}}/2)}{4 c_{\mathrm{s}} - D}. \tag{15}$$

Here the relation between the shock pressure P (given in the direct drive case by Eq. (1)), and the shock velocity in the target is:

$$D = \left(\frac{(\gamma + 1)}{2} \frac{P}{\rho_0} \right)^{1/2} \tag{16}$$

where γ is the adiabatic constant of the material at high pressure (this can be approximated by the value for a perfect gas, $\gamma \approx 1.67$). Instead the sound velocity c_{s} in the compressed material is

$$c_{\mathrm{s}} = \left(\gamma \frac{P}{\rho} \right)^{1/2} \tag{17}$$

In conclusion, this simple model allows to obtain the minimum ($d_{\min}$) and the maximum ($d_{\max}$) thickness of a target for which the shock is stationary.

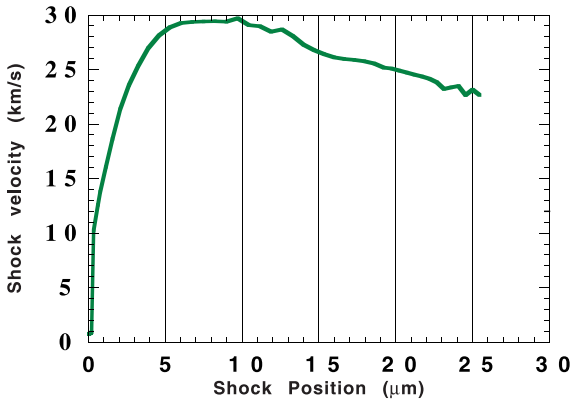

Fig. 7. Numerical simulation of the trend of the shock velocity *versus* target thickness obtained with the hydrodynamical code MULTI [28] for a laser intensity of 10^{14} W/cm^2 and an Al target.

In our experimental conditions, in the case of aluminium and with direct drive case ($I_{\mathrm{L}} \approx 10^{14}$ W/cm^2, $P \approx 16$ Mbar) we get $D_{\mathrm{Al}} \approx 28$ μm/ns and $c_{\mathrm{s}} \approx 16$ μm/ns. Now, in order to apply equations (11, 15) to evaluate $d_{\min}$ and $d_{\max}$ we need an estimate of the rise time t_{R} of the laser pulse and of t_{L}. Since our pulse has a Gaussian temporal shape with FWHM = 450 ps, we assumed, as a conservative estimate, that both the rise time of the laser pulse and the "stationary" phase last about 450 ps. By applying equations (11, 15) we then get $d_{\min} \approx 6$ μm and $d_{\max} \approx 22$ μm. Recalling that the typical thicknesses of targets used in our experiment were $\approx$10 μm for the base of the target and $\approx$16 μm for the total thickness of the aluminium target (base + step), the conditions for stationarity were satisfied.

1D hydrodynamical simulations performed with the code MULTI [28] substantially confirms these results although they take into account the actual (Gaussian) temporal shape of the laser pulse. Figure 7 shows the time behaviour of shock velocity obtained by hydrodynamical simulation for a peak laser intensity $I = 10^{14}$ W/cm^2.

Let's notice that Figure 7 shows how in the interval between 6 and 22 μm the shock velocity variation is less than 16%. Keeping in account the many approximations used in our model, the agreement is satisfactory.

We can deal with stationarity also in the case of indirect drive. In this case the ablation pressure should be calculated by using equation (4). In this case $P \approx t^{-3/26}$ (see Eq. (4)) while in direct drive $P \approx t^{-1/8}$. Therefore the indirect drive approach allows to obtain shocks which are (slightly) steadier. However indirect drive allows to obtain stationary shocks also with short laser pulses: while in direct drive, after the end of the laser pulse ($t > t_{\mathrm{L}}$), the relaxation wave is generated and the pressure starts to rapidly decrease (quicker than as $t^{-1/8}$), in indirect drive the cavity behaves as an "energy reservoir". The laser energy may be deposited in the cavity in a very short time, but then the pressure applied to the target decreases with the law $t^{-3/26}$, as a consequence of the dynamics of plasma and radiation inside the cavity [17].

6 Conclusions

In conclusion, this paper discusses in detail the quality requirements for EOS shock wave measurements, and shows how these have been satisfied in the experiment at Max Planck Institut für Quantenoptik. A planar shock is obtained using optical smoothing techniques in the direct drive or by the indirect drive approach.

The main causes of preheating in the direct drive approach can be eliminated by using a short wavelength laser and a sufficiently low intensity; also optical smoothing helps to reduce preheating. In our experiment, the main concern to preheating is due to X-rays: this is strongly reduced by using an appropriate target thickness and a CH layer on the laser side. In indirect drive, preheating can strongly be reduced by a careful design of the cavity geometry.

To avoid non-stationarity of the shock, an appropriate choice of target thickness is required, depending on the laser pulse duration and rise time.

We warmly acknowledge the support of the MPQ technical team. The experiment was realised at MPQ and supported by the E.U. in the framework of the program "Access to Large Scale Facilities".

References

1. P. Mora, Phys. Fluids **25**, 1051 (1982)
2. A. Caruso, R. Gratton, Plasma Phys. **10**, 867 (1968)
3. J. Lindl, Phys. Plasmas **2**, 3933 (1995)
4. Ya.B. Zeldovich, Yu.P. Raizer, *Physics of Shock Waves and High Temperature Hydrodinamic Phenomena* (Academic, New York, 1967)
5. A. Benuzzi *et al.*, Phys. Rev. E **54**, 2162 (1996)
6. D. Batani *et al.*, Phys. Rev. B **61**, 9287 (2000); M. Koenig, B. Faral, J.M. Boudenne, D. Batani, S. Bossi, A. Benuzzi, C. Remond, J. Perrine, M. Temporal, S. Atzeni, Phys. Rev. Lett. **74**, 2260 (1995); N.5, pp. R5927-R5930 (2000); D. Batani, A. Morelli, M. Tomasini, A. Benuzzi-Mounaix, B. Faral, M. Koenig, P. Baclet, B. Cathala, B. Marchet, I. Masclet, M. Rebec, Ch. Reverdin, R. Cauble, P. Celliers, G. Collins, L. Da Silva, T. Hall, M. Moret, B. Sacchi, Phys. Rev. Lett. **88**, 235502 (2002)
7. B. Faral *et al.*, "Fabrication des cibles bimarches", Rapport Scientifique LULI 1993, p. 309 (1994)
8. Y. Kato *et al.*, Phys. Rev. Lett. **53**, 1057 (1984)
9. R.M. Stevenson *et al.*, Opt. Lett. **19**, 363 (1994)
10. T.H. Bett *et al.*, Appl. Opt. **34**, 4025 (1995)
11. S. Dixit *et al.*, Appl. Opt. **32**, 2543 (1993)
12. D. Batani, F. Giugliano, T. Hall, M. Koenig, Phys. Rev. E **64**, 047401 (2001)
13. C. Bleu, D. Batani, Th. Löwer, Eur. Phys. J. D **19**, 231 (2002)
14. A. Benuzzi *et al.*, Phys. Rev. E **60**, R2488 (1999)
15. D. Batani, W. Nazarov, T. Hall, Th. Löwer, M. Koenig, A. Benuzzi, B. Faral, N. Grandjouan Phys. Rev. E **62**, 8573 (2000)
16. See for instance, Y. Aglitskiy, Th. Lehecka, S.P. Obenschain, S. Bodner, C.J. Pawley, K. Gerber, J. Sethian, C.M. Brown, J.F. Seely, U. Feldman, G.E. Holland, Use of spherically bent crystals for Nike-laser-plasma spectral diagnostics and monochromatic imaging, in *Applications of X Rays Generated from Lasers and Other Bright Sources*, edited by G.A. Kyrala, J.C. Gauthier, SPIE **3157**, 104, Bellingham, Washington (1997)
17. R. Sigel, *Laser-Plasma Interactions* (M.B. Hooper, SUSSP, Edinburgh, 1989), Vol. 4, p. 53
18. R.L. Kauffman *et al.*, Phys. Rev. Lett. **73**, 2320 (1994)
19. T. Hall *et al.*, Phys. Rev. E **55**, R6356 (1997)
20. Th. Löwer *et al.*, Phys. Rev. Lett. **72**, 3186 (1994)
21. A. Benuzzi *et al.*, Phys. Plasma **5**, 2410 (1998)
22. D. Batani *et al.*, Plasma Phys. Contr. Fus. **41**, 93 (1999)
23. H.A. Baldis, E.M. Campbell, W.L. Kruer, in *Handbook of Plasma Physics*, edited by M.N. Rosenbuth, R.Z. Sagdeev (North-Holland, Amsterdam, 1991), Vol. 3, Chap. 9
24. Th. Löwer, "Erzeugung von Multimegabar-Stobwellen in Festköpern durch lasererzeugte thermische Strahlung", Ph.D. thesis, Max-Planck Institut fr Quantenoptik, Garching, Germany, 1994
25. R. Fabbro *et al.*, Phys. Rev. **26**, 2289 (1982)
26. B. Henke, in *X-ray data booklet*, Center for X-ray optics (Lawrence Berkeley Laboratory, University of California, 1986)
27. M. Temporal *et al.*, Nuovo Cim. D **19**, 1839 (1997)
28. R. Ramis, R. Schmalz, J. Meyer-ter-Vehn, Comput. Phys. Comm. **49**, 475 (1988)
29. M. Koenig *et al.*, Phys. Rev. E **50**, R3314 (1994)